Engineering Research Journal
journal homepage: https://erj.journals.ekb.eg/

# Key Factors Affecting the Performance of Square Concrete-Filled Steel Tube Columns: A Comparative Analysis of International Design Codes

Mahmoud A. H. Abdullatif [1,*], Fattouh M. F. Shaker [1], Nehal M. Ayash [1] and Nabil Mansour [2]

[1]Civil Engineering Department, Faculty of Engineering Mataria, Helwan University
[2]Civil Engineering Department, Faculty of Engineering, Badr University in Cairo
[*]Corresponding author E-mail: mahmoudatef456@gmail.com

**Abstract.** This study utilizes finite element analysis (FEA) with ANSYS to validate the behavior of concrete-filled square steel tube (CFST) columns. Key findings indicate that concrete compressive strength significantly influences load capacity, with increases of up to 288% noted when strength rises from 25 MPa to 100 MPa, particularly for lower slenderness ratios. The impact of steel yield strength was less significant, especially in higher slenderness specimens that failed due to local buckling. Additionally, the study evaluates the provisions of international design codes, revealing that the ECP 205-2007 tend to overestimate axial loads, whereas the AISC 360-16-2016 code aligns more closely with FEA predictions.

**Keywords:** Square Concrete-Filled Steel Tubes, Finite Element Modeling, Nonlinear Analysis, Codes provisions, Failure Mechanisms

## 1 Introduction

Concrete-Filled Steel Tubular (CFST) structures represent a cutting-edge engineering advancement, merging the tensile strength and flexibility of steel with the compressive advantages of concrete. Prominently utilized in modern construction, CFSTs enhance overall structural integrity, offer superior fire resistance, and streamline the building process. The effectiveness of CFST columns stems from the composite action between the steel tube and concrete core. The steel tube enhances concrete's compressive strength, while the concrete prevents local buckling of the steel. CFSTs are extensively used in skyscrapers, bridges, and industrial buildings due to their material efficiency and outstanding performance under seismic and dynamic forces. This combination of materials results in robust, cost-efficient, and resilient infrastructure solutions. It has also been shown that CFST beams and columns show high stiffness and strength under flexural loads. In addition, CFST structures perform well in seismic conditions, maintaining strength and stiffness but with a quicker reduction in post-peak resistance.

The adoption of CFST in construction has been supported by the development of design codes, such as the Egyptian Code of Practice for Steel Construction ECP 205-2007 (LRFD) [1], Eurocode EN 1994-1-1-2004 [2], Australian/New Zealand standards AS/NZS 5100.6-2017 [3], Canadian CSA S16-14-2014 [4], and American AISC 360-16-2016 [5]. These codes standardize the design and analysis of CFST structures, by providing empirical formulas and simplified models for designing CFST columns and beams. These guidelines facilitate efficient and reliable design by considering material properties, dimensions, and load conditions. Advances in material science, including high-strength steel and concrete composites, have further improved CFST performance. Despite this progress, some standards still limit the strength of materials used in CFST, with ongoing research aimed at extending these limits, particularly in relation to Egyptian standards.

DOI: 10.21608/erj.2025.362558.1210
Received 23 March 2025; Received in revised form 22 May 2025; Accepted 04 June 2025
Available online 01 September 2025

Failure modes in CFST columns typically involve local buckling of the steel tube, crushing of the concrete core, or global buckling, with key factors being material properties, cross-sectional dimensions, and loading conditions. The following summary outlines the current state of research in CFSTs, covering key areas such as experimental testing results, finite element modeling, applications of high-strength concrete and steel, the impact of lateral restraint on concrete core behavior and local buckling of the steel section, as well reviewing current and proposed predictive design models.

Recent experimental and analytical studies on circular concrete-filled steel tubes (CFSTs) were conducted by **Deifalla et al.** and **Shaker et al.** [6], [7]. The experimental phase [6] involved testing 27 specimens with varying diameters, tube thicknesses, and heights, while ensuring that the selected *D/t* ratios mitigated the risk of local buckling. Two primary failure mechanisms were identified: yielding of the steel tube and global buckling of the members. Subsequent analytical research [7] utilized finite element modeling in ANSYS, calibrated against the experimental results from the earlier work [6]. This effort expanded the scope to include 64 models, broadening the range of experimental parameters. The research focused specifically on long circular CFST sections, where the global buckling was the dominant failure mode. Accordingly, the ANSYS models assumed full bond interaction between the steel tube and the concrete core. The findings indicated that CFST performance improves significantly with higher compressive concrete strengths, while increased steel yield strength showed minimal impact on the system's overall behavior.

Finite element analysis (FEA) has become essential for advancing our understanding of CFST performance under various conditions. **Ouyang and Kwan (2018)** [8] developed an FE model specifically for square CFST columns, achieving accurate predictions of axial compressive behavior validated against 92 specimen tests. Building on this, **Hassanein et al. (2017)** [9] introduced a design model tailored for hexagonal CFST columns, finding that larger diameters yielded notable performance improvements. **Patel and Lande (2016)** [10] further expanded FEA applications by examining both rectangular and circular CFST columns, identifying key parameters such as tube thickness and concrete grade as influential factors in column performance. Meanwhile, **Tao et al. (2013)** [11] refined FE modeling for CFST stub columns, underscoring the importance of precisely simulating the steel tube's passive confinement effect on the concrete core to improve prediction accuracy.

Concrete type and strength are central to CFST behavior. **Uy (2001)** [12] introduced a mixed analysis method to account for high-strength steel in these structures, while **Han** and **Yao (2004)** [13] found that Self-Compacting Concrete (SCC) achieves load-bearing capacity comparable to that of vibrated concrete, demonstrating SCC's potential for CFST applications. **Zhang** and **Guo (2004)** [14] highlighted the importance of maintaining balanced steel-to-concrete ratios to avoid local buckling and uphold structural integrity. Additionally, **Hernández-Figueirido et al. (2012)** [15] showed that high-strength concrete enhances load capacity, whereas normal-strength concrete provides the added benefit of greater ductility—critical for CFST performance. **Sakino et al. (2004)** [16] observed that higher-strength concrete boosts both load-bearing capacity and overall structural performance, while **Uy (2012)** [17] demonstrated that high-strength concrete enhances impact resistance and energy absorption. Moreover, recent advancements, such as ultra-high-performance concrete (UHPC) and specialized steel alloys, have further elevated CFST structural capabilities. For instance, **Yan et al. (2023)** [18] found that ultra-high-performance nano-concrete (UHPNC) reinforcements in CFST columns improve durability and load-bearing capacity. Their findings indicate that increasing UHPNC layer thickness and nano-silica content enhances both compressive strength and toughness, with experimental results aligning closely with a new formula for long-term predictions. **Liew et al. (2010)** [19] also tested configurations with ultra-high-strength concrete (UHSC) fillings, finding that while UHSC columns achieve significant load capacities, they exhibit brittleness after peak load; however, adding steel fibers effectively increases ductility and strength. Finally, **Han et al. (2014)** [20] emphasized the importance of accurate concrete placement techniques—such as pump and gravity filling—to ensure strength and compactness within hollow steel tubes. They further recommend maintaining a clean steel surface and incorporating vent holes to prevent bursting under fire exposure. **Khan et al. (2017)** [21] found that CFST sections—particularly those using high-strength steel and concrete—achieved full section capacity without reductions from local buckling, thus outperforming steel columns in structural performance.

**Liew and Xiong (2012)** [19] examined CFST columns with varying steel tube thicknesses and diameters, testing both ultra-high-strength concrete (UHSC) and normal-strength concrete (NSC) infills. Their results indicated that thicker steel tubes increase confinement and load-bearing capacity, though these benefits come with increased brittleness post-peak load, especially when the steel's contribution to overall strength is low. In related studies, **O'Shea and Bridge (2000)** [22] and **Johansson and Gylltoft (2002)** [23] observed that internal lateral restraints enhance buckling resistance in square CFST tubes, though this effect diminishes in circular tubes. Johansson further emphasized the importance of strain compatibility between the steel and concrete components, as misalignment can compromise structural resilience. **O'Shea and Bridge (2000)** [22] also investigated how CFST geometric properties affect stability. Their findings showed that columns with a high length-to-diameter ratio are more susceptible to global buckling, while an increased diameter-to-thickness ratio raises the risk of local buckling. They stressed that a well-bonded interface between steel and concrete is crucial for minimizing buckling and optimizing structural performance.

**Khan et al. (2017)** [21] [24] conducted experimental and finite element analyses on CFST sections incorporating high-strength steel (HSS) and high-strength concrete (HSC) and compared their results with code prescribed capacities. They found that existing design codes accurately predict the ultimate strengths of these sections, showing that CFST members can reach full load capacity without significant local buckling. When compared with standards such as AS4100 and AS5100.6,

the predicted strengths aligned closely with experimental data, confirming the applicability of these codes for high-strength CFSTs. **Giakoumelis and Lam (2004)** [25] concluded that Eurocode 4 offers the most precise predictions for high-strength CFSTs, while noting discrepancies in other codes that may affect accuracy. In a similar **vein, Varma et al. (2002)** [26] validated the accuracy of ACI codes in predicting moment capacity, further endorsing the reliability of established design guidelines for CFST applications. **Sakino et al. (2004)** [16] proposed predictive formulas for axial loads, identifying tube yield strength and local buckling as critical factors.

# 2 Objective

Previous research has primarily focused on circular CFST columns, with limited attention given to square sections. Additionally, there has been a limited number of studies comparing results with international codes. This study aims to address these gaps by conducting a verification study using the FE software ANSYS to compare experimental results on axially loaded CFST columns. The research will investigate the impact of various factors, including concrete compressive strength, steel yielding strength, length-to-width ratio, and length-to-thickness ratio. Furthermore, it will compare the FE results with several international codes, including ECP 205, AS/NZS, and AISC 360-16.

# 3 Finite Element Modeling and Verification

## 3.1 Verification Model Details

**Khan et al.** [17] conducted an experimental study on 6 square concrete-filled steel tube (CFST) column specimens that were subjected to a concentric load, which are provided in **Table 1**. Each test specimen is identified by its unique code name; CB15SH, can be explained as follows: CB refers to the composite section; 15 refers to the *b/t* ratio; SH refers to the short column. The end supports used for the tested specimens are fixed supports for the short columns, as shown in **Fig. 1**.

The steel tubes are considered as a High-strength Steel (HSS) material, which provided an average yield stress ($f_y$) of 762 MPa, an average modulus of elasticity ($E_s$) of 213,973 MPa, and an average ultimate strength ($f_u$) of 819 MPa. The infill concrete of specimens has an average compressive strength of 100 MPa and 113 MPa as High-strength Concrete (HSC), as shown in **Table 1**. The average modulus of elasticity ($E_c$) of the infill concrete is 44,880 MPa.

**Table 1** Details for the tested short columns' specimen by **Khan et al.** [21]

| No. | Specimen Label | Column width *b* (mm) | Tube thickness *t* (mm) | *b / t* | Column height *H*(mm) | *H / b* | Concrete compressive strength $f_c$ (MPa) |
|---|---|---|---|---|---|---|---|
| 1 | CB15SH | 75 | 5 | 15 | 285 | 3.8 | 100 |
| 2 | CB20SH | 100 | 5 | 20 | 360 | 3.6 | 100 |
| 3 | CB25SH | 125 | 5 | 25 | 435 | 3.48 | 100 |
| 4 | CB30SH | 150 | 5 | 30 | 510 | 3.4 | 100 |
| 5 | CB30SL1 | 150 | 5 | 30 | 1060 | 7.07 | 113 |
| 6 | CB40SL1 | 200 | 5 | 40 | 1060 | 5.3 | 113 |

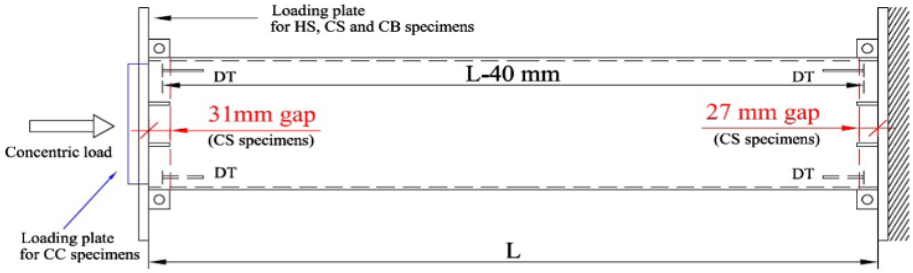


**Fig. 1** Fixed end conditions for short test specimens **Khan et al.** [21]

## 3.2 Analytical Model

### 3.2.1 Element Types

The above listed experimental results were modeled using ANSYS. The concrete core was modeled using the SOLID65 element, designed for 3D solids with or without reinforcing bars. This element allows for cracking in tension and crushing in compression and is defined by eight nodes with three translational degrees of freedom per node (x, y, and z directions). For the steel tube, the SOLID45 element was employed, also defined by eight nodes with three translational degrees of freedom, and well-suited for the 3D modeling of solid structures.

Loading and support plates were modeled with the SOLID185 element, an eight-node element with three translational degrees of freedom per node. SOLID185 is robust in handling plasticity, stress stiffening, creep, large deflections, and large strains, making it suitable for 3D modeling of solid structures.

To capture the contact interaction between the steel tube and the concrete infill, frictionless contact was achieved by CONTA174 and TARGE170 elements. CONTA174 models contact and slide between deformable surfaces and 3D "target" surfaces represented by TARGE170. This element is compatible with 3D structural analysis and conforms to the geometric characteristics of the solid or shell element it interfaces with, ensuring accurate simulation of the composite behavior of steel and concrete. See **Figures (2 – 6)**.

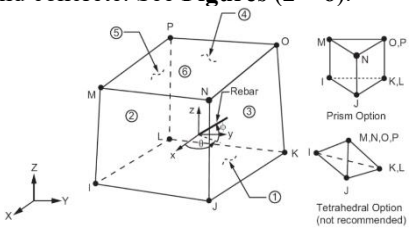


**Fig. 2** SOLID65 geometry

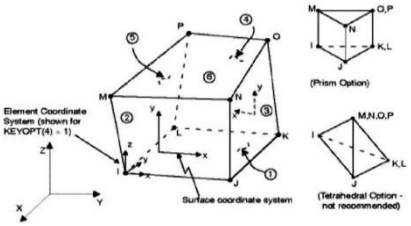


**Fig. 3** SOLID45 geometry

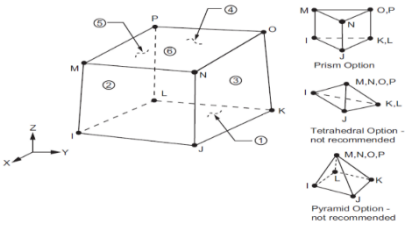


**Fig. 4** SOLID185 geometry

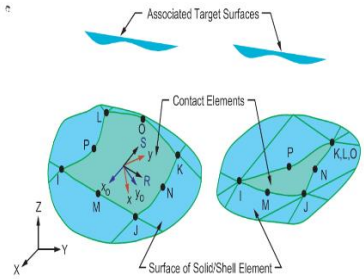


**Fig. 5** CONTA174 geometry

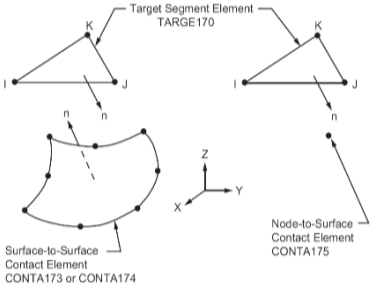


**Fig. 6** TARGE170 geometry

### 3.2.2 Material Properties

#### 3.2.2.1 Steel tube

Steel tubes of the SOLID45 element type need to be defined using both linear and multilinear isotropic materials. For linear characteristics, Poisson's ratio and EX represent the steel modulus of elasticity. The multilinear isotropic functions were developed using the steel stress-strain curve, with the initial modulus of elasticity $E_s$ being 0.1 and the strain hardening modulus $E_t$ (from the yielding stage to the final stage) to be 0.1. **Fig. 8** represents the stress-strain curve for steel tube (based on experimental study by **Khan et al.** [21]).

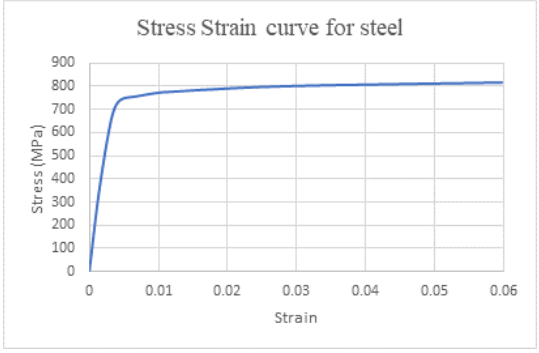


**Fig. 7** Stress-strain curve for steel tube (based on experimental study by **Khan et al.** [21])

### 3.2.2.2 Infilled concrete:

When concrete is subjected to laterally confining pressure, the uniaxial compressive strength $f'_{cc}$ and the corresponding strain ($\varepsilon_{cc}$), as shown in **Fig. 8**, are much higher than those of unconfined concrete $f'_c$. **Yu et al.** [27] stated that the relations between $f'_{cc}$ and $f'_c$ is given by:

$$f'_{cc} = [2+0.6 \ln (\boldsymbol{\zeta})] \, . \, f'_c \quad \ldots\ldots\ldots\ldots\ldots\ldots [1]$$

where: $f'_{cc}$ = Confined concrete strength, $f'_c$ = Characteristic compressive concrete strength, $\boldsymbol{\zeta}$ = confinement factor = $\frac{As.\ fy}{Ac.\ f'_c}$, $A_s$ = Steel cross-sectional area, $A_c$ = Concrete cross-sectional area, and $f_y$ = Yield strength of steel.

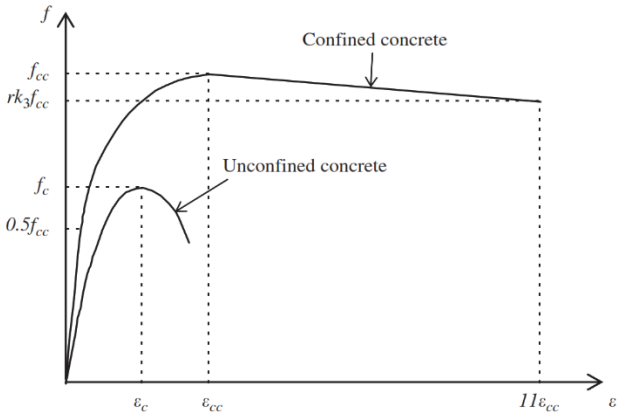


**Fig. 8** Equivalent uniaxial stress-strain curve for confined and unconfined concrete. [28]

The values of confined concrete strength $f'_{cc}$ for tested columns are listed in **Table 2** and shown in **Fig. 9**.

**Table 2** Material properties of concrete infill (based on experimental study by **Khan et al.** [21])

| No. | Specimen Label | $A_S$ (mm) | $A_C$ (mm) | $f'_{cc}$ (MPa) |
|---|---|---|---|---|
| 1 | CB15SH | 1380 | 4096 | 241 |
| 2 | CB20SH | 1900 | 8100 | 221 |
| 3 | CB25SH | 2380 | 12996 | 207 |
| 4 | CB30SH | 2900 | 19600 | 195.2 |
| 5 | CB30SL1 | 2900 | 19600 | 214.5 |
| 6 | CB40SL1 | 3900 | 36100 | 194.7 |

The concrete infill is defined using the SOLID65 element, which requires both linear and multilinear isotropic material properties. Following Hu [29], the modulus of elasticity, $E_{cc}$, for the concrete was calculated as $E_{cc} = 4700\sqrt{f'_{cc}}$, with Poisson's ratio used for the linear properties. The stress–strain curve of the concrete was employed to define the multilinear isotropic functions. This compressive stress–strain relationship consists of two distinct parts: the first part represents the linear zone, up to a stress level of 0.5 $f'_{cc}$; the second part models the elastic–plastic zone, reaching the maximum compressive stress of the concrete. This maximum compressive stress is obtained from the stress relationship as described in the following equation:

$$f = \frac{E_{cc}\,\varepsilon}{1+(R+R_E-2)(\varepsilon/\varepsilon_{cc})-(2R-1)(\varepsilon/\varepsilon_{cc})^2+R(\varepsilon/\varepsilon_{cc})^3} \quad \ldots\ldots\ldots\ldots\ldots\ldots [2]$$

where $R_E$ and R values are calculated from the following equations:

$$R_E = \frac{E_{cc}\,\varepsilon_{cc}}{f'_{cc}} \quad \ldots\ldots\ldots\ldots\ldots\ldots [3]$$

$$R = \frac{R_E\,(R_\sigma-1)}{(R_\varepsilon-1)^2} - \frac{1}{R_\varepsilon} \quad \ldots\ldots\ldots\ldots\ldots\ldots [4]$$

While the constants $R_\sigma$ and $R_\varepsilon$ are taken equal to 4 as recommended by **Hu** [29].

Also, the strain at the ultimate compressive strength is $\varepsilon_{cc}$ and can be calculated from the following equation:

$$\varepsilon_{cc} = \varepsilon_c \left(1 + k_2 \frac{f_l}{f'_c}\right) \quad \ldots\ldots\ldots\ldots\ldots\ldots [5]$$

While the factor $k_2$ is taken as 20.5 as recommended by **Hu et al.** [29].

Where $f_l$ is the lateral confining pressure imposed by the steel tube, and can be calculated from the following equation:

$$f_l/f_y = 0.055048 - 0.001885\,(B/t) \quad \ldots\ldots\ldots\ldots\ldots\ldots [6]$$

The end point of the curve is defined at $f'_{cc}$ and $\varepsilon_{cc}$. In addition, the uniaxial cracking stress was determined using $f_{ctr} = 0.6\sqrt{f'_{cc}}$ .

It is required to specify the appropriate values of shear transfer in cases of open and closed cracks. The values of the open and closed shear transfer coefficients are between 0 and 1.0. The value of the closed shear transfer coefficient must be greater than the value of the open shear transfer coefficient. Several preliminary analyses were attempted with various values for the shear transfer coefficient within a range equal to 0.1 to 0.2 for open cracks, and 0.7 to 1 for closed cracks up to no deviation of results is observed. Therefore, the shear transfer coefficients for the open and closed cracks used in this study were equal to 0.2 and 0.9, respectively.

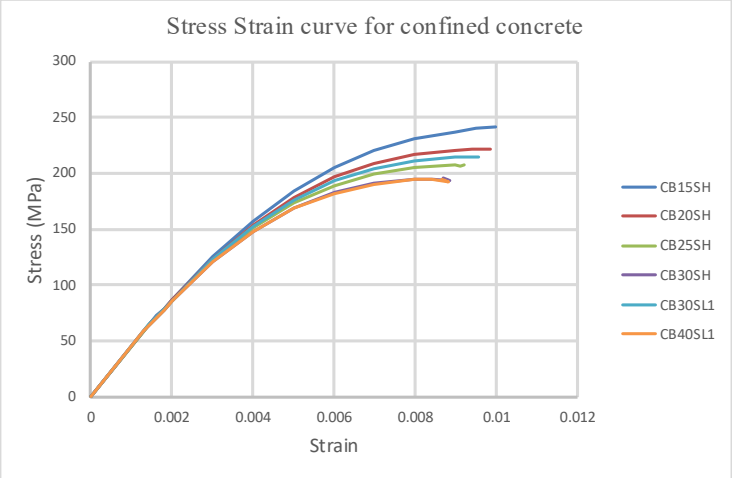


**Fig. 9** Stress-strain curve for confined concrete infill used in F.E. Modeling

### 3.2.2.3 Loading and supporting plates:

The loading and supporting steel plates are defined using the SOLID185 element type, which also requires both linear and multilinear isotropic material properties. For the linear properties, EX is set to 200,000 MPa, while PRXY is assumed to be 0.3.

### 3.2.3 Modeling

The volumes of the columns and loading plates were used as the basis for modeling. CFST column models were created with various heights, ranging from 285 mm to 1060 mm. Tube column widths spanned 74 mm to 200 mm, with a consistent wall thickness of 5 mm. Stiffeners positioned at the column ends had cross-sectional dimensions of 30 mm by 30 mm, with a 5 mm thickness. The loading and supporting steel plates were also modeled with 30 mm thickness. **Fig. 11** illustrates one of the tube column models created using ANSYS software.

### 3.2.4 Meshing, Boundary Conditions, and Loading:

A sensitivity study was conducted to identify the optimal element type and mesh configuration for modeling the steel tube elements of the CFST. Various mesh arrangements and sizes were tested to determine the most effective layout. The performance of each FE model was assessed by comparing its load-deformation behavior against experimental results.

Through this study, a fine 8-node SOLID45 brick element mesh with a balanced element size was found to achieve a good correlation with experimental results while remaining time-efficient. Using hex-mapped meshing with an element size of *B*/10 (where *B* is the column width) yielded accurate results and efficient computation, as illustrated in **Fig. 10**. As shown, the failure load predictions for the three mesh sizes are nearly identical: the *B*/5 model shows a 1% increase, and the *B*/20 model shows a 2% increase over the *B*/10 model. This study also noted that increasing the mesh size could increase analysis time by nearly five times compared to the *B*/10 model, a critical factor when running multiple models in the parametric study.

The sensitivity study revealed that the optimal mesh configuration consisted of a fine layout featuring a single element through the thickness of the steel tube member, modeled with 8-node SOLID45 brick elements. The loading end plates, both top and bottom, were represented using 8-node SOLID185 brick elements, while the infill concrete was modeled with 8-node SOLID65 brick elements. This arrangement produced the best correlation with the experimental load-deformation response, see **Fig. 11 (a) and (b)**.

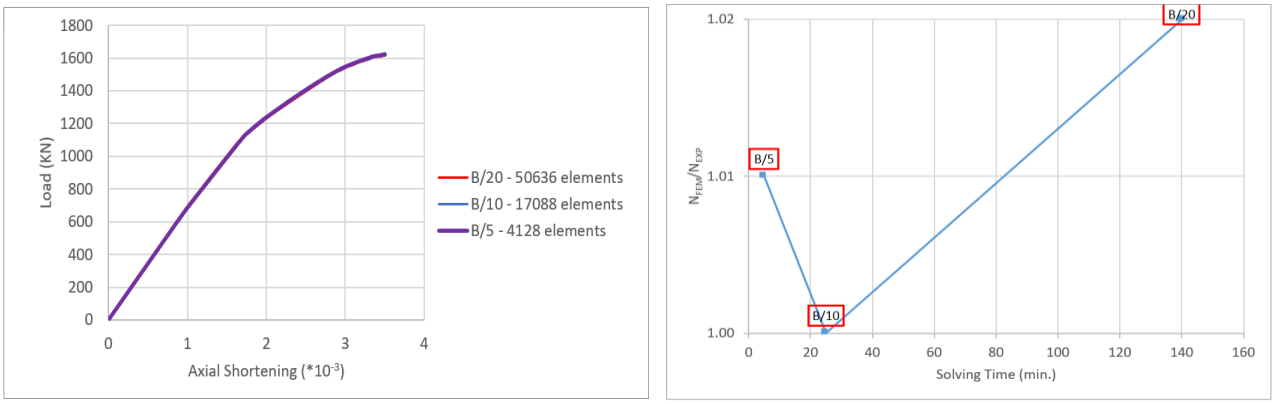


(a) (b)

**Fig. 10** Mesh sensitivity study (a) load-axial shortening curve (b) Ratio between failure load from ANSYS and experimental

A vertical and concentric load was applied to the columns as a concentrated load at the nodes. The displacement boundary conditions were established to constrain the column supports according to two setups, reflecting the configurations of the experimental testing machine. In the setup designed for short columns with heights up to 660 mm, the degrees of freedom (DOF) at all nodes at the bottom of the column were constrained as follows: Ux, Uy, Uz = 0. At the top of the column, the constraints were Ux, Uz = 0 but Uy was free in the loading direction. This configuration simulates a fixed-base restraint at the bottom of the column and a hinged restraint at the top, as represented in **Fig. 11 (c)**.

To accurately simulate the interaction between the inner surface of the steel tube and the outer surface of the infill concrete in the composite sections, a surface-to-surface frictionless contact was employed. This approach is crucial for identifying certain modes of failure that may not be detected when assuming a complete bond between the concrete infill and the steel tube, particularly in the case of short columns. Such failures can include out-of-plane local buckling of the steel tube, which can occur due to separation between the steel and concrete surfaces. If full contact or full bond is assumed, this type of failure may go unnoticed until the concrete infill fails, which does not align with the observed experimental behavior. Contact and target elements are shown in **Fig. 11 (d) and (e)**.

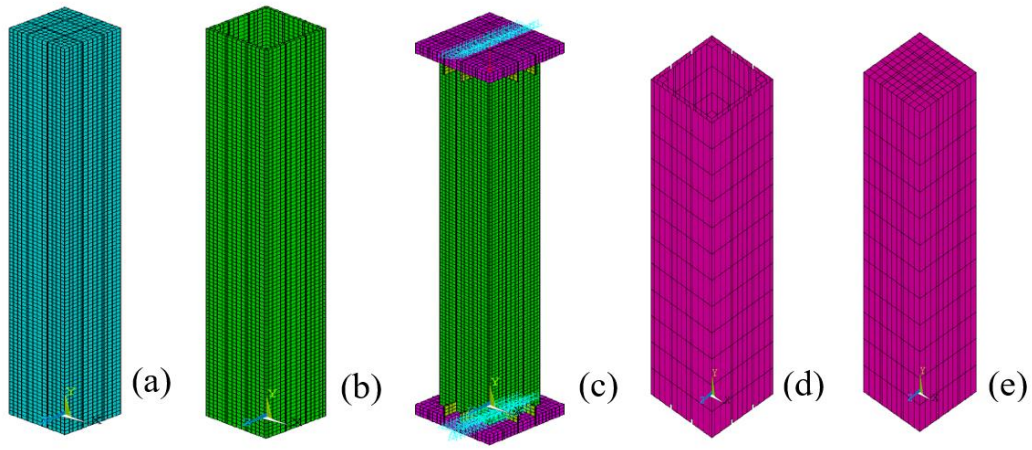


**Fig. 11** The meshing of CFST columns (a) Concrete core (SOLID65) (b) Steel tube (SOLID45) (c) Full Model with the degree of freedom restraints and load application; (d) contact element and (e) target element.

### 3.2.5 Analysis Type

The nonlinear static analysis was conducted using the Full Newton–Raphson method, incorporating a sufficiently large number of sub-steps during the loading process. This approach allows for accurate capturing of critical behaviors, including cracking in the concrete, yielding in the steel tube, as well as buckling and ultimate failure stages. A convergence tolerance of 0.001 was established based on the applied force *F*. The typical commands utilized for the nonlinear static analysis are outlined in **Table 3**.

**Table 3** Commands used to control nonlinear static analysis

| Type of analysis | Static |
|---|---|
| Analysis Options | Large Displacement Static |
| Calculate prestress effects | Yes |
| Time at end of load step | 10,000,000 |
| Automatic time stepping | On |
| Time step size | 1,000 |
| Min time step | 100 |
| Max time step | 10,000 |
| Frequency | Write every sub-step |
| Write items to result file | All solution items |

### 3.2.6 Results of Verification Study:

Von Mises stresses are utilized to compare the failure modes between the finite element models developed using ANSYS and the experimental specimens tested by **Khan** [17], as illustrated in **Fig. 12**. The results indicate that the finite element models successfully capture the failure mechanisms and the associated deformed shapes of the tested specimens. This includes the local failure in the short columns. As demonstrated in these figures, the locations of failure in the finite element models, indicated by the maximum values of Von Mises stresses, align well with the observed failures in the experimental tests.

The comparisons between the failure loads obtained from the experimental tests and the finite element models generated by ANSYS are presented in **Table 4**. Notably, the difference in failure loads between the analytical results and the experimental specimens ranged from +3% to -3%. **Fig. 13** illustrates the load-axial shortening comparison between the FEM and experimental results, demonstrating an acceptable convergence in the load-axial shortening relationships. Thus, the nonlinear finite element models for the CFST columns developed using ANSYS can be confidently utilized for further parametric studies.

**Table 4** Comparison between the failure load experimentally and analytically

| No. | Specimen Label | By **Khan et al.** [21] | | By Authors | $\frac{N_{FEM}}{N_{EXP}}$ |
|---|---|---|---|---|---|
| | | **Experimental Load** $N_{Exp}$ **(kN)** | **Failure Mode** | **FEM Load** $N_{FEM}$ **(kN)** | |
| 1 | CB15SH | 1755 | Local | 1700 | 0.97 |
| 2 | CB20SH | 2520 | Local | 2475 | 0.98 |
| 3 | CB25SH | 3023 | Local | 3100 | 1.03 |
| 4 | CB30SH | 4115 | Local | 4250 | 1.03 |
| 5 | CB30SL1 | 4833 | Local | 4890 | 1.01 |
| 6 | CB40SL1 | 7506 | Local | 7400 | 0.99 |
| **Average** | | | | | **1.00** |

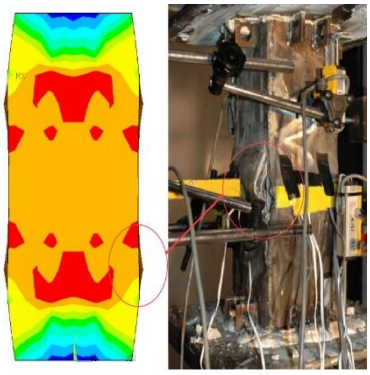

CB20SH

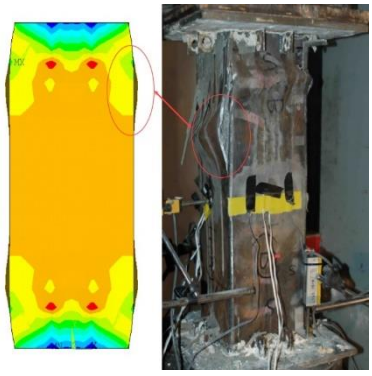

CB30SH

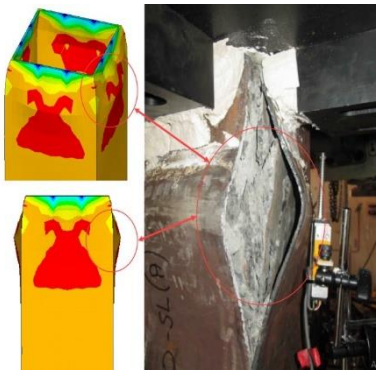

CB40SL1

**Fig. 12** Failure modes comparison between FEM and Experimental results

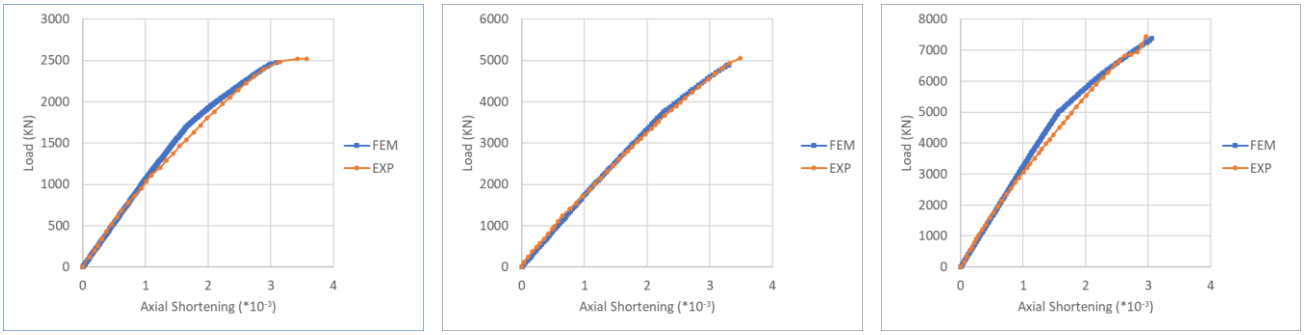


(a) CB20SH (b) CB30SL1 (c) CB40SL1

**Fig. 13** Load-Axial Shortening comparison between FEM and Experimental results

# 4 Parametric study

Following the calibration study conducted using ANSYS software to simulate the performance of CFST columns, Finite Element (FE) analysis was employed with similar procedures to explore various parameters. A total of thirty – six (36) different finite element models of CFST columns were created and examined, each varying in specific parameters. This research investigated a range of parameters, including:

1. Concrete compressive strength ($f_{cu}$) taken as 25, 40, and 100 MPa.
2. Steel yielding strength ($f_y$) taken as 235, 355, and 690 MPa.
3. Length-to-thickness ratio ($L/t$) "Local slenderness" and taken as 30, 55, 69, and 92.

These values were selected to ensure the validity of the study as the following:

1. The concrete minimum typical strength is 25 MPa, and maximum is 100 MPa.
2. S235 and S355 are common steel yield strengths. S690 is included to check if codes equations are valid for high strength steel.
3. $L/t$ values were obtained from comparing several code local buckling limits.
4. The $H/B$ was fixed equal to 5 for this study to ensure that all specimens are short.

Each test specimen is assigned to a unique code name that conveys key information about its properties. For instance, the code C25-S235-1-30 can be interpreted as follows: C denotes the concrete compressive strength ($f_{cu}$) of 25 MPa; S indicates the steel yield strength ($f_y$) of 235 MPa; and 30 refers to the length-to-thickness ratio ($L/t$). The data for the specimens used in parametric study, along with the results, are summarized in **Table 14**. The dimensions of the CFST columns are defined as: $H$ = height of the columns, $B$ = breadth of the columns, $L$ = length of the columns, and $t$ = thickness of the steel plates.

## 4.1 Effect of Concrete compressive strength ($f_{cu}$)

The behavior of CFST columns was investigated using concrete with varying compressive strengths of 25, 40, and 100 MPa. **Fig. 14** illustrates the influence of concrete compressive strength ($f_{cu}$) on the failure load of CFST columns, considering different local slenderness ratios (length-to-thickness ratio ($L/t$)).

The results demonstrate that concrete compressive strength has a significant and pronounced impact on the strength of CFST columns. Specifically, increasing the compressive strength from 25 MPa to 100 MPa led to an average increase in load capacity ranging from 178% to 288% for $L/t$ = 30, 244% to 333% for $L/t$ = 55, 260% to 341% for $L/t$ = 69, and 242% to 321% for $L/t$ = 92.

Furthermore, the impact of increasing concrete compressive strength ($f_{cu}$) on the load capacity of CFST columns with a steel yielding strength ($f_y$) of 235 MPa is less pronounced in specimens with a steel yielding strength of 690 MPa. This discrepancy arises because the steel samples with $f_y$ = 690 MPa can sustain loads without failure until the concrete reaches its compressive strength. In contrast, steel samples with $f_y$ = 235 MPa tend to fail before the concrete attains its compressive strength.

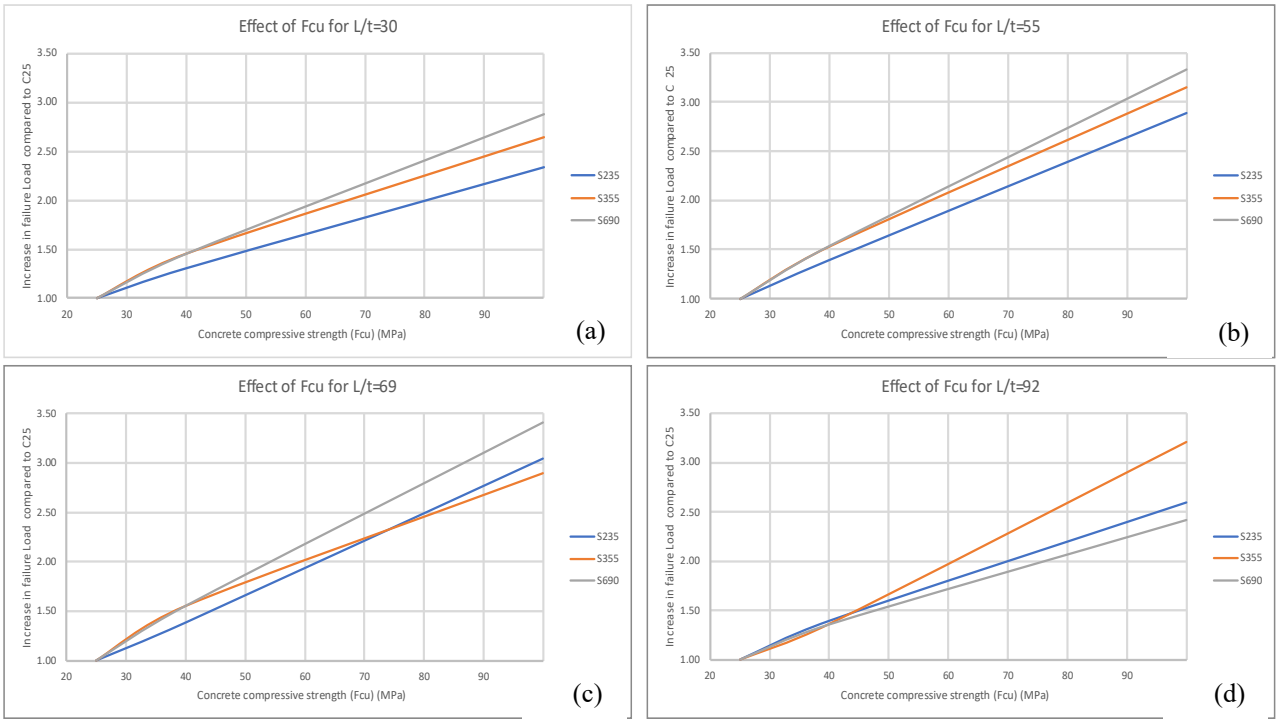


**Fig. 14** Effect of concrete compressive strength ($f_{cu}$) on the failure load of the CFST

## 4.2 Effect of Steel yielding strength ($f_y$)

The behavior of CFST columns was examined using steel with varying yielding strengths of 235, 355, and 690 MPa. The impact of steel yielding strength ($f_y$) on the failure load of CFST columns, considering different values of local slenderness (length-to-thickness ratio, $L/t$), is presented in **Fig. 15**. It is observed that the influence of steel yielding strength ($f_y$) on CFST strength is less significant than that of concrete compressive strength ($f_{cu}$).

Increasing the steel yielding strength ($f_y$) from 235 MPa to 690 MPa resulted in an average change in load capacity of (95%-139%) for $L/t$ = 30, (99%-123%) for $L/t$ = 55, (100%-118%) for $L/t$ = 69, and (98%-110%) for $L/t$ = 92. Notably, the increase in load capacity is greatest for specimens with $L/t$ = 30 and diminishes with an increasing $L/t$ ratio, reaching the lowest increase in capacity for specimens with $L/t$ = 92. This trend occurs because a higher $L/t$ ratio causes specimens to fail due to local buckling rather than yielding, thereby minimizing the benefits of utilizing steel with higher yield strength.

**Fig. 15 (d)** indicates that the specimen with a concrete compressive strength ($f_{cu}$) of 100 MPa and a length-to-thickness ratio ($L/t$) of 92 exhibits results that deviate from the trend observed in the other samples. This inconsistency may be attributed to the steel contribution ratio ($\delta$) of approximately 0.12, which is below the minimum steel contribution ratio of 0.2 recommended for CFST by the Eurocode (EN 1994-1-1, 2004) [2]. Additionally, the effect of increasing steel yielding strength ($f_y$) on the load capacity of CFST columns with a concrete compressive strength ($f_{cu}$) of 25 MPa is less pronounced in specimens with $f_{cu}$ = 100 MPa. This is because the concrete samples with $f_{cu}$ = 100 MPa can sustain loads without failure until the steel reaches its maximum strength, while those with $f_{cu}$ = 25 MPa tend to fail before the steel attains its maximum strength. Similarly, those with $f_{cu}$ = 40 MPa tend to yield for sections with low steel grades.

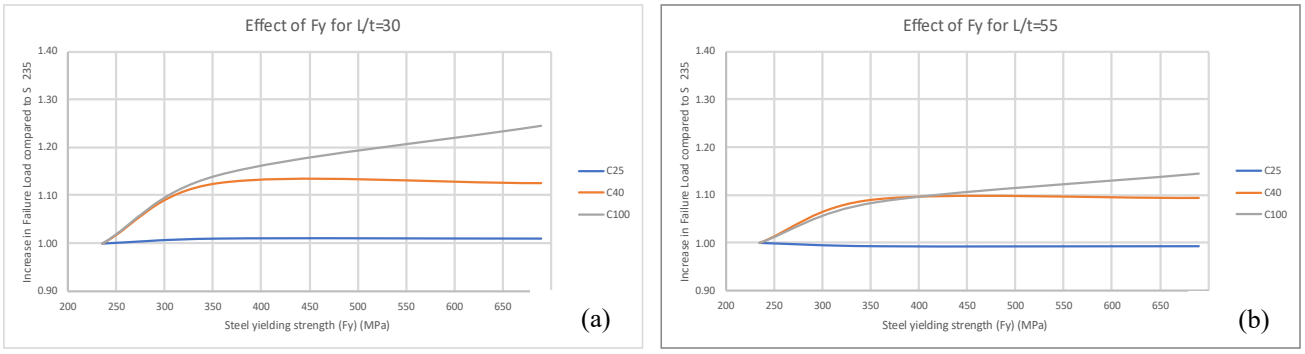

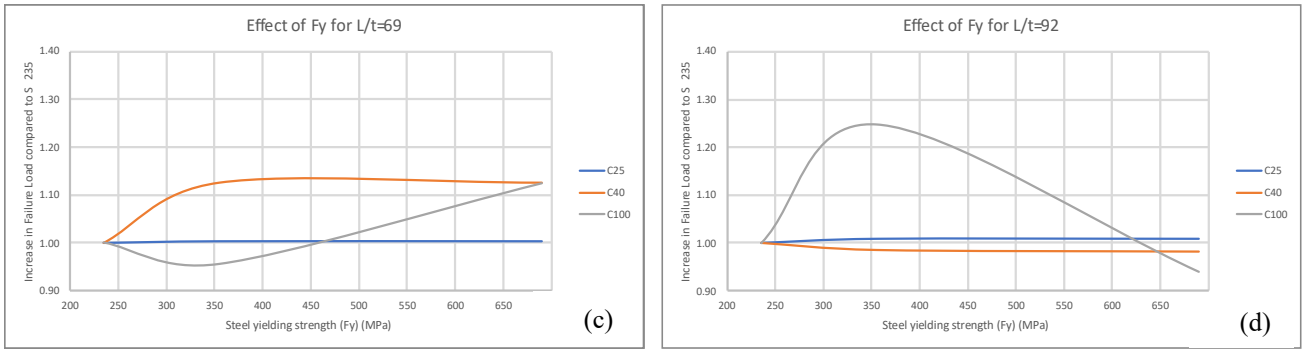


**Fig. 15** Effect of steel yielding strength ($f_y$) on the failure load of the CFST

## 4.3 Effect of Length-to-thickness ratio (*L/t*) "Local slenderness"

The behavior of CFST columns was studied using samples with various length-to-thickness ratios (*L/t*), specifically 30, 55, 69, and 92. The effect of the length-to-thickness ratio (*L/t*) on the failure load of the CFST is presented in **Fig. 16**. The findings indicate that local slenderness (*L/t*) significantly influences the strength of the CFST. As the length-to-thickness ratio increases from 30 to 92, the load capacity decreases by an average of (50%-73%). **Fig. 16** illustrates that a higher local slenderness ratio causes the specimens to fail due to local buckling before reaching their yield strength.

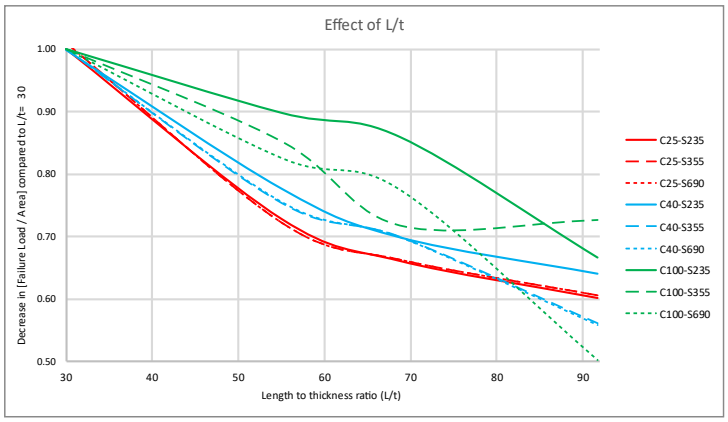


**Fig. 16** Effect of length-to-thickness ratio on the failure load of the CFST

# 5 Different international design codes

A comparative analysis was performed among five international codes governing the design of concrete-filled steel tube (CFST) sections. The design loads prescribed by these various codes were evaluated against the failure loads obtained from finite element modeling (FEM). This paper presents comparisons of three design codes:

1. The Egyptian Code of Practice for Steel Construction - Load and Resistance Factor Design "ECP 205-2007 (LRFD)" [1].
2. The Australian/New Zealand standards for steel and composite construction "AS/NZS 5100.6-2017" [3].
3. The American Institute of Steel Construction Specification for Structural Steel Buildings "AISC 360-16-2016" [5].

## 5.1 Comparison between FEM results and different codes:

The results obtained from Finite Element Method (FEM) analysis were compared with those predicted by various design codes across different structural configurations. This comparison aims to evaluate the accuracy and reliability of the design codes in predicting structural behavior, particularly when employing high-strength concrete and steel sections, and for CFST sections having local slenderness ratios outside code limits. The axial loads derived analytically from ANSYS and those obtained from the different design codes are presented in **Table 15** and illustrated in **Fig. 17**.

The comparison between the average load capacity ratios ($P_{CODE}$ / $P_{FEM}$) for various design codes provides valuable insights into their respective performances. Notably, the ECP 205 (LRFD) exhibits a ratio of 127%, suggesting the highest overestimation of load capacity compared to FEM results. In contrast, the AS/NZS demonstrates a ratio of 115%, implying a relatively closer agreement with FEM results. While AISC presents only a 9% overestimation of load capacity, which is the closest to FEM results.

The analysis of load capacity comparison ratios ($P_{CODE}$ / $P_{FEM}$) reveals notable variations influenced by steel yielding stress. Across different yielding stresses, certain trends emerge regarding the performance of the design codes. Specimens with steel yielding stresses of 235 MPa and 355 MPa consistently show better agreement with FEM results compared to those with a yielding stress of 690 MPa. For instance, the ECP 205 (LRFD) exhibits ratios of 102%, 114%, and 166% for steel yielding stresses of 235 MPa, 355 MPa, and 690 MPa, respectively, indicating a trend of overestimation with increasing yielding stress. The AS/NZS similarly overestimates load capacity across different yielding stresses, with ratios of 104%, 108%, and 133% for steel yielding stresses of 235 MPa, 355 MPa, and 690 MPa, respectively. Conversely, the AISC shows mixed performance; it underestimates axial loads for 235 MPa with a ratio of 96%, while for 355 MPa and 690 MPa, it overestimates with ratios of 103% and 127%, respectively.

It is important to note that steel with a yielding stress of 690 MPa exceeds the limitations set by most codes, except for AS/NZS. Interestingly, specimens with a yielding stress of 690 MPa show better ratios when combined with 100 MPa concrete. AS/NZS yields a ratio of 114%, which is the only code that accommodates these values for steel yielding strength and concrete compressive strength.

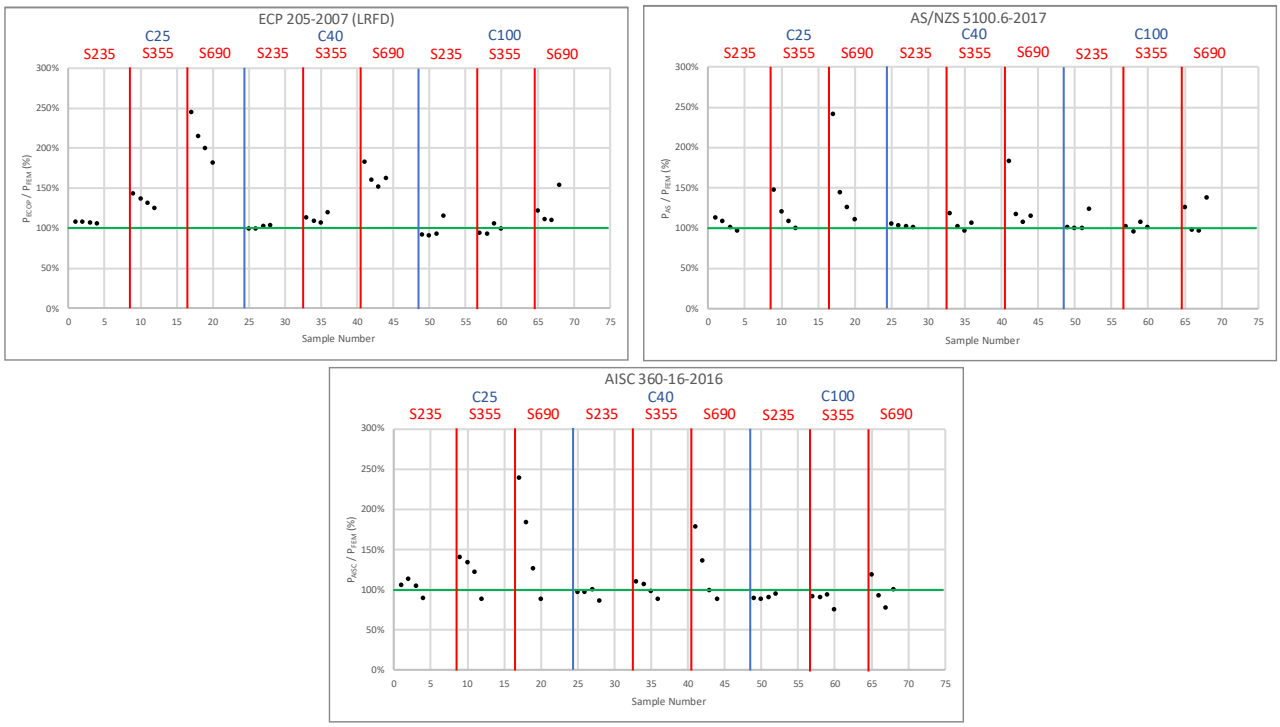


**Fig. 17** Comparison between different codes and FEM results

## 5.2 Comparison between FEM results and different codes for specimens within the limits:

Each design code has its unique set of limitations when considering steel-yielding strength, concrete compressive strength, and the prevention of local buckling. While these codes provide essential guidelines for structural design, they are inherently constrained by their assumptions and methodologies. **Tables 5 and 6** show the codes limitations for local slenderness ratio ($L/t$) to consider the local buckling effects and values of concrete compressive strength and steel-yielding strength respectively.

**Table 5** Codes limitations for local slenderness ratio ($L/t$) to consider the local buckling effects.

| Code | Codes Limitations | | Codes Limitations for different yielding strengths ($F_y$) (MPa) | |
|---|---|---|---|---|
| ECP | To avoid Local Buckling | $\sqrt{3Es/fy}$ | S235 | 51.3 |
| | | | S355 | 41.7 |
| | | | S690 | N/A |
| AS/AISC | Compact/Non-Compact Limit | | S235 | 66.9 |

| | | | | |
|---|---|---|---|---|
| | | $2.26\sqrt{Es/fy}$ | S355 | 54.4 |
| | | | S690 **(AS)** | 39.0 |
| | | | S690 **(AISC)** | N/A |
| | Non-Compact/Slender Limit | $3\sqrt{Es/fy}$ | S235 | 88.8 |
| | | | S355 | 72.2 |
| | | | S690 **(AS)** | 51.8 |
| | | | S690 **(AISC)** | N/A |

**Table 6** Codes limitations for values of concrete compressive strength and steel-yielding strength.

| Code | Max. concrete compressive strength (MPa) | Max. steel yielding strength (MPa) |
|---|---|---|
| ECP | 40 | --- |
| AS | 100 | 690 |
| AISC | 69 | 525 |

### 5.2.1 ECP 205-2007 (LRFD):

The specimens that fulfill the limitations of ECP 205-2007 (LRFD) for concrete compressive strength, steel yielding strength, and to avoid happening of local buckling are shown in **Table 7** and **Fig. 18.**
The specimens falling within the prescribed limits of ECP 205-2007 (LRFD) exhibit an average ratio of $P_{ECOP}/P_{FEM}$ at 116%, indicating an overestimation of the failure load for CFST according to ECP 205-2007 (LRFD) guidelines. This observation aligns with previous findings, demonstrating a consistent trend. Notably, specimens featuring a steel yielding strength of 235MPa consistently yield results with higher conformity compared to those with a yielding strength of 355MPa. Furthermore, even among specimens with a steel yielding strength of 355MPa, those filled with concrete having a compressive strength of 40MPa demonstrate greater conformity compared to counterparts with a compressive strength of 25MPa.

**Table 7** Comparison between FEM results and ECP 205-2007 (LRFD):

| | | $P_{ECP}$ (kN) | $P_{ECP}/P_{FEM}$ |
|---|---|---|---|
| 1 | C25-S235-1-30-5 | 1031 | 108% |
| 5 | C25-S355-1-30-5 | 1383 | 143% |
| 13 | C40-S235-1-30-5 | 1234 | 99% |
| 17 | C40-S355-1-30-5 | 1586 | 113% |
| | | **Average** | **116%** |

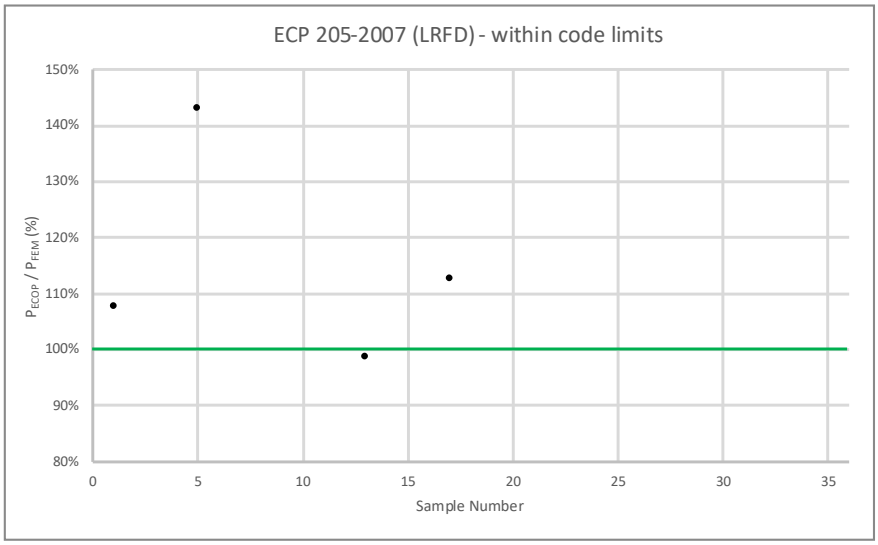


**Fig. 18** Comparison between FEM results and ECP 205-2007 (LRFD)

### 5.2.2 AS/NZS 5100.6-2017:

The specimens that fulfill the limitations of AS/NZS 5100.6-2017 for concrete compressive strength, steel yielding strength, and characterized to compact, non-compact, and slender sections according to AS/NZS 5100.6-2017 classifications are shown in **Tables (8, 9, and 10)** and **Figures (19, 20, and 21),** together with the comparison between $P_{AS}/P_{FEM}$ for compact, non-compact, and slender sections respectively. It should be noted that AS/NZS 5100.6-2017 is the only code that considers sections with steel yielding strength reaching up to 690MPa.

The specimens falling within the prescribed limits of AS/NZS 5100.6-2017 exhibit an average ratio of $P_{AS}/P_{FEM}$ at 129% for compact sections, 107% for non-compact sections, and 110% for slender sections indicating an overestimation of the failure load for CFST according to AS/NZS 5100.6-2017 guidelines. This observation aligns with previous findings, demonstrating a consistent trend for the effect of steel yielding strength and concrete compressive strength. Of interest is that slender sections give results with greater conformity compared to non-compact sections. When comparing the specimens with steel yielding strengths 235MPa, and 355MPa only, they exhibit better conformity with the code results with an average ratio of $P_{AS}/P_{FEM}$ at 110% for compact sections, 104% for non-compact sections, and 101% for slender sections.

**Table 8** Comparison between FEM results and AS/NZS 5100.6-2017 for compact sections

| | | $P_{AS}$ (kN) | $P_{AS}/P_{FEM}$ |
|---|---|---|---|
| 1 | C25-S235-1-30-5 | 1074 | 112% |
| 2 | C25-S235-1-55-5 | 2519 | 108% |
| 13 | C40-S235-1-30-5 | 1309 | 105% |
| 14 | C40-S235-1-55-5 | 3361 | 103% |
| 25 | C100-S235-1-30-5 | 2250 | 101% |
| 26 | C100-S235-1-55-5 | 6732 | 100% |
| 5 | C25-S355-1-30-5 | 1422 | 147% |
| 17 | C40-S355-1-30-5 | 1657 | 118% |
| 29 | C100-S355-1-30-5 | 2598 | 102% |
| 9 | C25-S690-1-30-5 | 2330 | 241% |
| 21 | C40-S690-1-30-5 | 2565 | 182% |
| 33 | C100-S690-1-30-5 | 3506 | 126% |
| | | **Average** | **129%** |

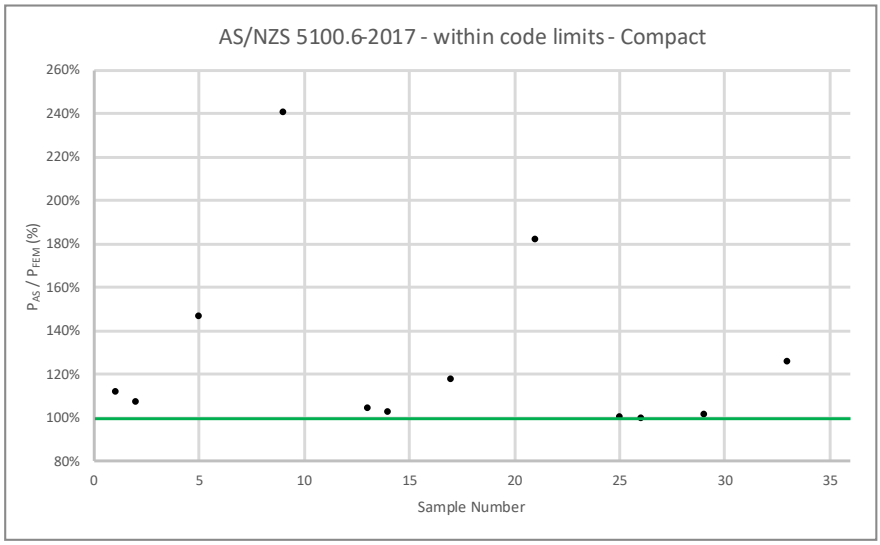


**Fig. 19** Comparison between FEM results and AS/NZS 5100.6-2017 for compact sections

**Table 9** Comparison between FEM results and AS/NZS 5100.6-2017 for non-compact sections

| | | $P_{AS}$ (kN) | $P_{AS}/P_{FEM}$ |
|---|---|---|---|
| 3 | C25-S235-1-69-5 | 2139 | 101% |
| 15 | C40-S235-1-69-5 | 2994 | 102% |
| 27 | C100-S235-1-69-5 | 6416 | 99% |
| 6 | C25-S355-1-55-5 | 2781 | 120% |
| 7 | C25-S355-1-69-5 | 2306 | 108% |
| 18 | C40-S355-1-55-5 | 3623 | 102% |
| 19 | C40-S355-1-69-5 | 3162 | 96% |
| 30 | C100-S355-1-55-5 | 6994 | 95% |
| 31 | C100-S355-1-69-5 | 6584 | 107% |
| 10 | C25-S690-1-55-5 | 3342 | 144% |
| 22 | C40-S690-1-55-5 | 4185 | 117% |
| 34 | C100-S690-1-55-5 | 7556 | 98% |
| | | **Average** | **107%** |

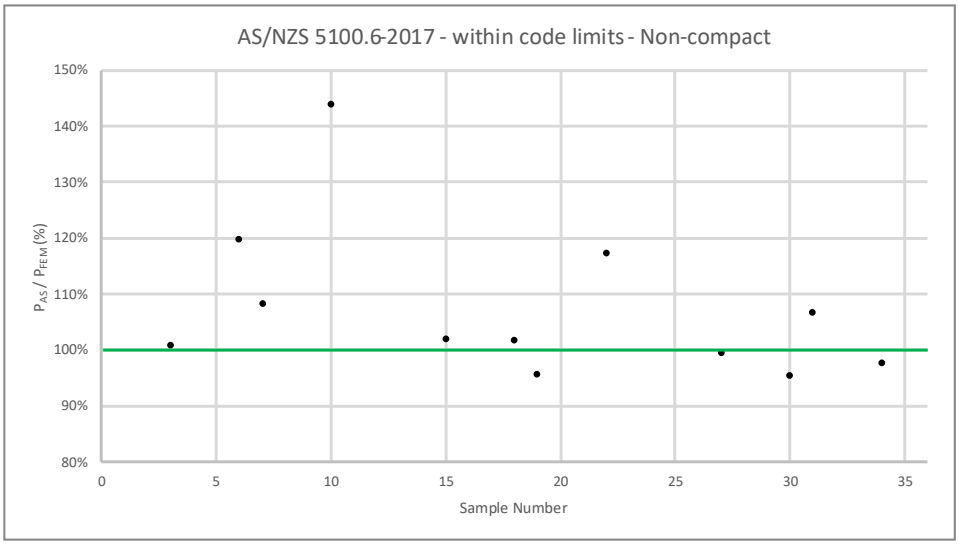


**Fig. 20** Comparison between FEM results and AS/NZS 5100.6-2017 for non-compact sections

**Table 10** Comparison between FEM results and AS/NZS 5100.6-2017 for slender sections

| | | $P_{AS}$ (kN) | $P_{AS}/P_{FEM}$ |
|---|---|---|---|
| 4 | C25-S235-1-92-5 | 1848 | 96% |
| 16 | C40-S235-1-92-5 | 2717 | 101% |
| 28 | C100-S235-1-92-5 | 6190 | 124% |
| 8 | C25-S355-1-92-5 | 1943 | 100% |
| 20 | C40-S355-1-92-5 | 2811 | 106% |
| 32 | C100-S355-1-92-5 | 6284 | 101% |
| 11 | C25-S690-1-69-5 | 2666 | 125% |
| 12 | C25-S690-1-92-5 | 2145 | 110% |
| 23 | C40-S690-1-69-5 | 3522 | 107% |
| 24 | C40-S690-1-92-5 | 3013 | 114% |
| 35 | C100-S690-1-69-5 | 6943 | 96% |
| 36 | C100-S690-1-92-5 | 6487 | 138% |
| | | **Average** | **110%** |

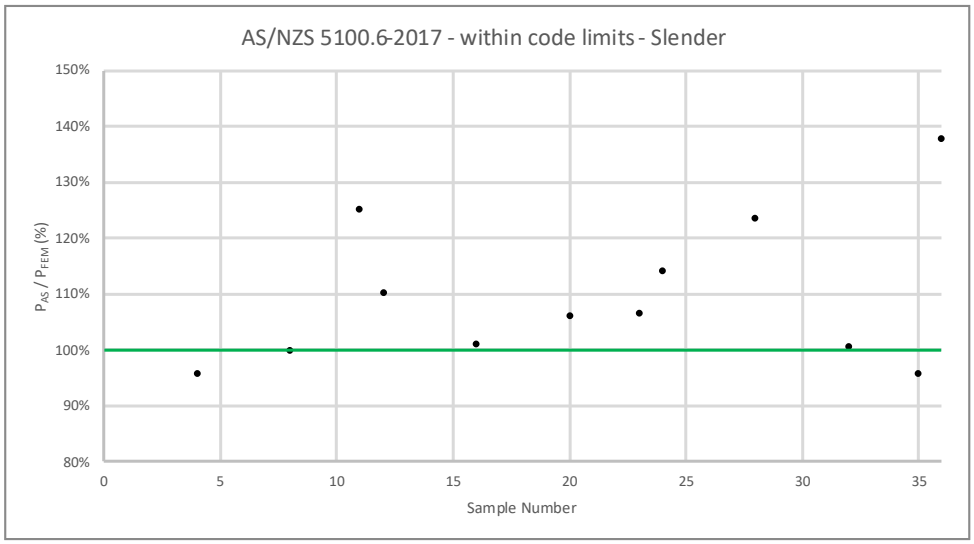


**Fig. 21** Comparison between FEM results and AS/NZS 5100.6-2017 for slender sections

### 5.2.3 AISC 360-16-2016:

The specimens that fulfill the limitations of AISC 360-16-2016 for concrete compressive strength, steel yielding strength, and characterized to compact, non-compact, and slender sections according to AISC 360-16-2016 classifications are shown in **Tables (11, 12, and 13)** and **Figures (22, 23, and 24)**, together with the comparisons between $P_{AISC}/P_{FEM}$ for compact, non-compact, and slender sections respectively.

The specimens falling within the prescribed limits of AISC 360-16-2016 exhibit an average ratio of $P_{AISC}/P_{FEM}$ at 111% for compact sections, 111% for non-compact sections, and 88% for slender sections indicating an overestimation of the failure load for CFST according to AISC 360-16-2016 guidelines for compact and non-compact sections. However, it indicates an underestimation for slender section. Notably, AISC 360-16-2016 is the only code for slender sections that underestimates the failure load compared to FEM results.

Overall, AISC 360-16-2016 yielded results that were the most consistent with the FEM results and this is a result of using an accurate classification for the sections according to the local buckling to compact, non-compact, and slender sections with different equations for calculating the failure load for each of them using different reduction factors depending on the accurate limit state of design.

**Table 11** Comparison between FEM results and AISC 360-16-2016 for compact sections

| | | $P_{AISC}$ (kN) | $P_{AISC}/P_{FEM}$ |
|---|---|---|---|
| 1 | C25-S235-1-30-5 | 1011 | 106% |
| 2 | C25-S235-1-55-5 | 2652 | 113% |
| 13 | C40-S235-1-30-5 | 1209 | 97% |

| | | | |
|---|---|---|---|
| 14 | C40-S235-1-55-5 | 3163 | 97% |
| 5 | C25-S355-1-30-5 | 1356 | 140% |
| 17 | C40-S355-1-30-5 | 1554 | 110% |
| | | **Average** | **111%** |

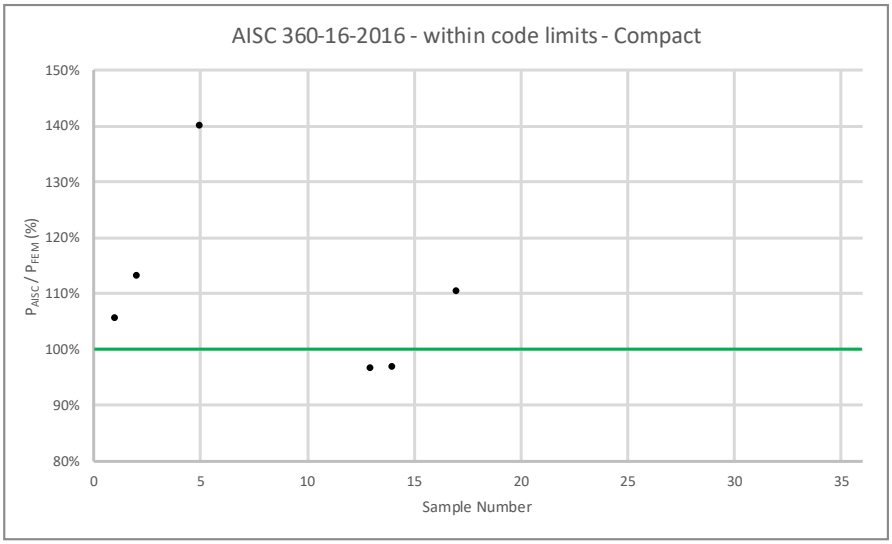


**Fig. 22** Comparison between FEM results and AISC 360-16-2016 for compact sections

**Table 12** Comparison between FEM results and AISC 360-16-2016 for non-compact sections

| | | $P_{AISC}$ (kN) | $P_{AISC}/P_{FEM}$ |
|---|---|---|---|
| 3 | C25-S235-1-69-5 | 2219 | 105% |
| 15 | C40-S235-1-69-5 | 2939 | 100% |
| 6 | C25-S355-1-55-5 | 3094 | 133% |
| 7 | C25-S355-1-69-5 | 2599 | 122% |
| 18 | C40-S355-1-55-5 | 3803 | 107% |
| 19 | C40-S355-1-69-5 | 3237 | 98% |
| | | **Average** | **111%** |

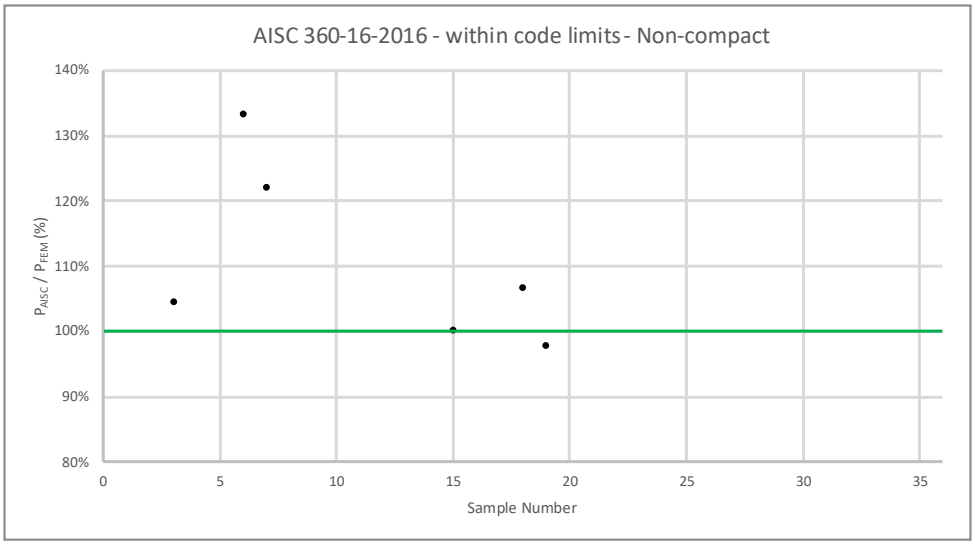


**Fig. 23** Comparison between FEM results and AISC 360-16-2016 for non-compact sections

**Table 13** Comparison between FEM results and AISC 360-16-2016 for slender sections

| | | $P_{AISC}$ (kN) | $P_{AISC}/P_{FEM}$ |
|---|---|---|---|
| 4 | C25-S235-1-92-5 | 1725 | 89% |
| 8 | C25-S355-1-92-5 | 1725 | 89% |
| 16 | C40-S235-1-92-5 | 2328 | 86% |
| 20 | C40-S355-1-92-5 | 2328 | 88% |
| | | **Average** | **88%** |

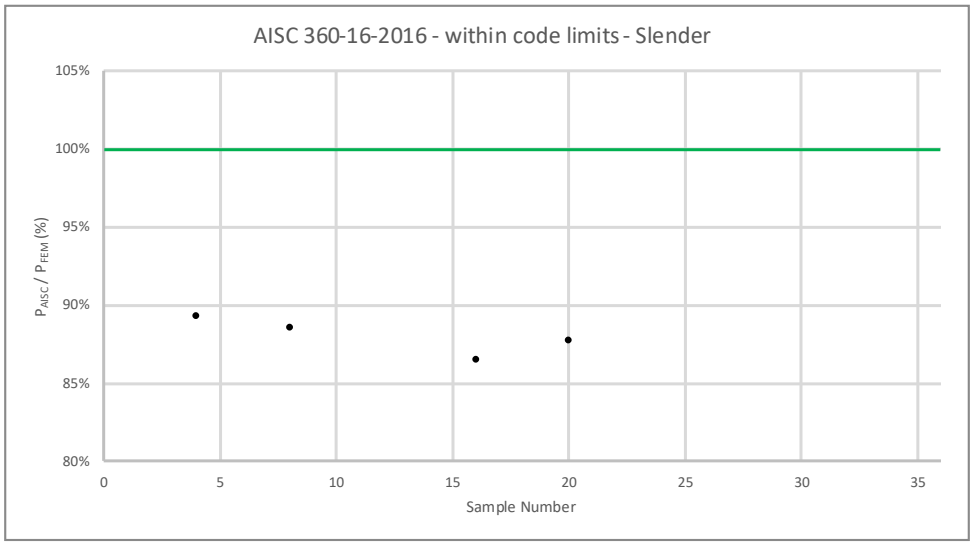


**Fig. 24** Comparison between FEM results and AISC 360-16-2016 for slender sections

# 6 Conclusions

The study has yielded several critical insights into the behavior of Square Concrete-Filled Steel Tubular (SCFST) columns under concentric axial loading. The primary observations are summarized below:

1. Concrete compressive strength ($f_{cu}$) is the most influential parameter affecting load capacity. Increasing $f_{cu}$ significantly boosts load capacity, especially in specimens with high yielding strength of steel tube ($f_y$ = 690 MPa). The results suggest that higher-compressive strength of infill concrete in conjunction with high-yielding strength steel tube contributes more effectively to the overall performance of CFST columns.
2. Steel yielding strength has a lesser impact on load capacity compared to concrete compressive strength. However, the enhancement effect of increasing the steel yielding strength of tube is most noticeable for columns with lower slenderness ratio ($L/t$= 30), where higher $f_y$ markedly increases the load capacity of CFST columns. This advantage diminishes for columns with higher $L/t$ ratios, as local buckling becomes the dominant failure mechanism.
3. The load capacity drops by an average of 50% to 73% as the length-to-thickness ratio rises from 30 to 92.
4. ECP 205-2007 (LRFD) overestimates the load capacity of SCFST columns with an average ratio of 127% compared to FEM results. AS/NZS 5100.6-2017 provides predictions with ratio 115%. AISC 360-16-2016 demonstrates the closest alignment with FEM results, overestimating by only 9%.
5. For all studied Standards/Codes the load capacity estimations for specimens with lower yielding strength steel tube ($f_y$ = 235 MPa and 355 MPa) aligned better with FEM results than those with highest yielding strength ($f_y$ = 690 MPa).
6. AISC 360-16-2016 was unique in its underestimation for slender sections, highlighting the complexities associated with accurately predicting behavior in this category.
7. AISC 360-16-2016 provided the most reliable results due to its detailed section classification and tailored equations for failure load calculations. This code highlights the importance of adapting design standards to account for local buckling and other nuanced interactions.

**Table 14** Data for specimens and FEM results

| | | $f_{cu}$ MPa | $f_y$ MPa | $B$ mm | $L$ mm | $t$ mm | $H$ mm | $L/t$ | Steel Contribution Ratio ($\delta$) | Failure Load (kN) | Max Stress MPa | | Steel Failure | Concrete Failure |
|---|---|---|---|---|---|---|---|---|---|---|---|---|---|---|
| | | | | | | | | | | | Steel | Concrete | | |
| 1 | C25-S235-1-30 | 25 | 235 | 150 | 150 | 5 | 750 | 30 | 0.63 | 957 | 199.2 | 20.5 | L.B | NO L.F. |
| 2 | C25-S235-1-55 | | | 275 | 275 | 5 | 1375 | 55 | 0.47 | 2340 | 183.6 | 20.5 | L.B | NO L.F. |
| 3 | C25-S235-1-69 | | | 275 | 275 | 4 | 1375 | 69 | 0.42 | 2123 | 179.8 | 20.6 | | NO L.F. |
| 4 | C25-S235-1-92 | | | 275 | 275 | 3 | 1375 | 92 | 0.35 | 1932 | 198.4 | 20.5 | | NO L.F. |
| 5 | C25-S355-1-30 | | 355 | 150 | 150 | 5 | 750 | 30 | 0.72 | 967 | 197.6 | 19.4 | | NO L.F. |
| 6 | C25-S355-1-55 | | | 275 | 275 | 5 | 1375 | 55 | 0.58 | 2322 | 186.2 | 20.4 | | NO L.F. |
| 7 | C25-S355-1-69 | | | 275 | 275 | 4 | 1375 | 69 | 0.52 | 2131 | 186 | 20.4 | | NO L.F. |
| 8 | C25-S355-1-92 | | | 275 | 275 | 3 | 1375 | 92 | 0.44 | 1947 | 187.7 | 20.7 | | NO L.F. |
| 9 | C25-S690-1-30 | | 690 | 150 | 150 | 5 | 750 | 30 | 0.83 | 967 | 197.6 | 19.4 | | NO L.F. |
| 10 | C25-S690-1-55 | | | 275 | 275 | 5 | 1375 | 55 | 0.73 | 2322 | 186.2 | 20.4 | | NO L.F. |
| 11 | C25-S690-1-69 | | | 275 | 275 | 4 | 1375 | 69 | 0.68 | 2131 | 186 | 20.5 | | NO L.F. |
| 12 | C25-S690-1-92 | | | 275 | 275 | 3 | 1375 | 92 | 0.61 | 1947 | 187.7 | 20.7 | | NO L.F. |
| 13 | C40-S235-1-30 | 40 | 235 | 150 | 150 | 5 | 750 | 30 | 0.52 | 1250 | 247.7 | 40 | Y | C.F. |
| 14 | C40-S235-1-55 | | | 275 | 275 | 5 | 1375 | 55 | 0.36 | 3266 | 245.5 | 40 | | C.F. |
| 15 | C40-S235-1-69 | | | 275 | 275 | 4 | 1375 | 69 | 0.31 | 2937 | 245.1 | 32.8 | | NO L.F. |
| 16 | C40-S235-1-92 | | | 275 | 275 | 3 | 1375 | 92 | 0.25 | 2692 | 276.9 | 40 | | C.F. |
| 17 | C40-S355-1-30 | | 355 | 150 | 150 | 5 | 750 | 30 | 0.62 | 1407 | 262 | 35.5 | L.B | NO L.F. |
| 18 | C40-S355-1-55 | | | 275 | 275 | 5 | 1375 | 55 | 0.46 | 3563 | 253.6 | 34.9 | | NO L.F. |
| 19 | C40-S355-1-69 | | | 275 | 275 | 4 | 1375 | 69 | 0.40 | 3307 | 251.8 | 35 | | NO L.F. |
| 20 | C40-S355-1-92 | | | 275 | 275 | 3 | 1375 | 92 | 0.33 | 2652 | 229.3 | 40 | | C.F. |
| 21 | C40-S690-1-30 | | 690 | 150 | 150 | 5 | 750 | 30 | 0.76 | 1407 | 264.4 | 32.9 | | NO L.F. |
| 22 | C40-S690-1-55 | | | 275 | 275 | 5 | 1375 | 55 | 0.62 | 3573 | 254.9 | 37.6 | | NO L.F. |
| 23 | C40-S690-1-69 | | | 275 | 275 | 4 | 1375 | 69 | 0.57 | 3307 | 253.2 | 35 | | NO L.F. |
| 24 | C40-S690-1-92 | | | 275 | 275 | 3 | 1375 | 92 | 0.49 | 2643 | 227.3 | 40 | | C.F. |
| 25 | C100-S235-1-30 | 100 | 235 | 150 | 150 | 5 | 750 | 30 | 0.30 | 2237 | 270.8 | 86.4 | Y | NO L.F. |
| 26 | C100-S235-1-55 | | | 275 | 275 | 5 | 1375 | 55 | 0.18 | 6752 | 269.9 | 93.1 | | NO L.F. |
| 27 | C100-S235-1-69 | | | 275 | 275 | 4 | 1375 | 69 | 0.16 | 6461 | 282.5 | 95.2 | | D.C. |
| 28 | C100-S235-1-92 | | | 275 | 275 | 3 | 1375 | 92 | 0.12 | 5011 | 342.8 | 84.4 | | D.C. |
| 29 | C100-S355-1-30 | | 355 | 150 | 150 | 5 | 750 | 30 | 0.40 | 2556 | 380.7 | 89.3 | | NO L.F. |
| 30 | C100-S355-1-55 | | | 275 | 275 | 5 | 1375 | 55 | 0.25 | 7327 | 376.5 | 92.8 | | NO L.F. |
| 31 | C100-S355-1-69 | | | 275 | 275 | 4 | 1375 | 69 | 0.21 | 6171 | 369 | 80.4 | | NO L.F. |
| 32 | C100-S355-1-92 | | | 275 | 275 | 3 | 1375 | 92 | 0.17 | 6249 | 420.4 | 100 | | C.F. |
| 33 | C100-S690-1-30 | | 690 | 150 | 150 | 5 | 750 | 30 | 0.56 | 2787 | 431.8 | 97.6 | L.B | D.C. |
| 34 | C100-S690-1-55 | | | 275 | 275 | 5 | 1375 | 55 | 0.40 | 7735 | 401.8 | 90 | | NO L.F. |
| 35 | C100-S690-1-69 | | | 275 | 275 | 4 | 1375 | 69 | 0.34 | 7261 | 438.1 | 90.3 | | D.C. |
| 36 | C100-S690-1-92 | | | 275 | 275 | 3 | 1375 | 92 | 0.28 | 4711 | 329.8 | 74 | | D.C. |

**Hints: L.B.** = Local Buckling, **Y**= Yielding, **D.C.**= Distorted Concrete, **C. F.** = Concrete Failure, and **NO L.F.** = No Local Failure

**Table 15** Comparison between different codes and FEM results

| | | $P_{FEM}$ | ECP 205-2007 (LRFD) [1] | | AS/NZS 5100.6-2017 [3] | | AISC 360-16-2016 [5] | |
|---|---|---|---|---|---|---|---|---|
| | | (kN) | $P_{ECOP}$ (kN) | $P_{ECOP}/P_{FEM}$ | $P_{AS}$ (kN) | $P_{AS}/P_{FEM}$ | $P_{AISC}$ (kN) | $P_{AISC}/P_{FEM}$ |
| 1 | C25-S235-1-30 | 957 | 1031 | 108% | 1074 | 112% | 1011 | 106% |
| 2 | C25-S235-1-55 | 2340 | 2502 | 107% | 2519 | 108% | 2652 | 113% |
| 3 | C25-S235-1-69 | 2123 | 2266 | 107% | 2139 | 101% | 2219 | 105% |
| 4 | C25-S235-1-92 | 1932 | 2029 | 105% | 1848 | 96% | 1725 | 89% |
| 5 | C25-S355-1-30 | 967 | 1383 | 143% | 1422 | 147% | 1356 | 140% |
| 6 | C25-S355-1-55 | 2322 | 3158 | 136% | 2781 | 120% | 3094 | 133% |
| 7 | C25-S355-1-69 | 2131 | 2793 | 131% | 2306 | 108% | 2599 | 122% |
| 8 | C25-S355-1-92 | 1947 | 2425 | 125% | 1943 | 100% | 1725 | 89% |
| 9 | C25-S690-1-30 | 967 | 2362 | 244% | 2330 | 241% | 2314 | 239% |
| 10 | C25-S690-1-55 | 2322 | 4982 | 215% | 3342 | 144% | 4258 | 183% |
| 11 | C25-S690-1-69 | 2131 | 4258 | 200% | 2666 | 125% | 2683 | 126% |
| 12 | C25-S690-1-92 | 1947 | 3528 | 181% | 2145 | 110% | 1725 | 89% |
| 13 | C40-S235-1-30 | 1250 | 1234 | 99% | 1309 | 105% | 1209 | 97% |
| 14 | C40-S235-1-55 | 3266 | 3228 | 99% | 3361 | 103% | 3163 | 97% |
| 15 | C40-S235-1-69 | 2937 | 3003 | 102% | 2994 | 102% | 2939 | 100% |
| 16 | C40-S235-1-92 | 2692 | 2776 | 103% | 2717 | 101% | 2328 | 86% |
| 17 | C40-S355-1-30 | 1407 | 1586 | 113% | 1657 | 118% | 1554 | 110% |
| 18 | C40-S355-1-55 | 3563 | 3883 | 109% | 3623 | 102% | 3803 | 107% |
| 19 | C40-S355-1-69 | 3307 | 3529 | 107% | 3162 | 96% | 3237 | 98% |
| 20 | C40-S355-1-92 | 2652 | 3172 | 120% | 2811 | 106% | 2328 | 88% |
| 21 | C40-S690-1-30 | 1407 | 2564 | 182% | 2565 | 182% | 2511 | 178% |
| 22 | C40-S690-1-55 | 3573 | 5705 | 160% | 4185 | 117% | 4841 | 135% |
| 23 | C40-S690-1-69 | 3307 | 4992 | 151% | 3522 | 107% | 3276 | 99% |
| 24 | C40-S690-1-92 | 2643 | 4274 | 162% | 3013 | 114% | 2328 | 88% |
| 25 | C100-S235-1-30 | 2237 | 2043 | 91% | 2250 | 101% | 2002 | 89% |
| 26 | C100-S235-1-55 | 6752 | 6124 | 91% | 6732 | 100% | 5996 | 89% |
| 27 | C100-S235-1-69 | 6461 | 5942 | 92% | 6416 | 99% | 5809 | 90% |
| 28 | C100-S235-1-92 | 5011 | 5759 | 115% | 6190 | 124% | 4732 | 94% |
| 29 | C100-S355-1-30 | 2556 | 2394 | 94% | 2598 | 102% | 2345 | 92% |
| 30 | C100-S355-1-55 | 7327 | 6777 | 92% | 6994 | 95% | 6632 | 91% |
| 31 | C100-S355-1-69 | 6171 | 6466 | 105% | 6584 | 107% | 5782 | 94% |
| 32 | C100-S355-1-92 | 6249 | 6152 | 98% | 6284 | 101% | 4732 | 76% |
| 33 | C100-S690-1-30 | 2787 | 3370 | 121% | 3506 | 126% | 3300 | 118% |
| 34 | C100-S690-1-55 | 7735 | 8593 | 111% | 7556 | 98% | 7170 | 93% |
| 35 | C100-S690-1-69 | 7261 | 7924 | 109% | 6943 | 96% | 5643 | 78% |
| 36 | C100-S690-1-92 | 4711 | 7250 | 154% | 6487 | 138% | 4732 | 100% |
| **Average** | | | | **127 %** | | **115 %** | | **109 %** |

# References

[1] Egyptian code of practice for steel construction (load and resistance factor design) Code No. (205)- Ministerial Decree No. 359-2007-first edition. 2008.
[2] Eurocode 4, Design of composite steel and concrete structures. Part 1-1: general rules and rules for building, European Committee for Standardization,. 2004.
[3] "Standards Australian AS5100.6. Bridge design, Part 6: steel and composite construction," 2017.
[4] Canadian Standards Association (CSA). Design of Steel Structures. S16-14 Mississauga (Ontario, Canada). 2014.
[5] American Institute of Steel Construction (AISC). Specification for Structural Steel Buildings. ANSI/AISC360-16, Chicago (IL, USA). 2016.
[6] A. F. Deifalla, F. M. Fattouh, M. M. Fawzy, and I. S. Hussein, "Behavior of stiffened and unstiffened CFT under concentric loading, An experimental study," Steel Compos. Struct. An Int. J., vol. 33, no. 6, pp. 793–803, 2019.
[7] F. M. F. Shaker, M. S. Daif, A. F. Deifalla, and N. M. Ayash, "Parametric study on the behavior of steel tube columns with infilled concrete—An analytical study," Sustainability, vol. 14, no. 21, p. 14024, 2022.
[8] Y. Ouyang and A. K. H. Kwan, "Finite element analysis of square concrete-filled steel tube (CFST) columns under axial compressive load," Eng. Struct., vol. 156, pp. 443–459, 2018.
[9] M. F. Hassanein, V. I. Patel, and M. Bock, "Behaviour and design of hexagonal concrete-filled steel tubular short columns under axial compression," Eng. Struct., vol. 153, pp. 732–748, 2017.
[10] V. Patel and P. S. Lande, "Analytical behavior of concrete filled steel tubular columns under axial compression," Int. J. Eng. Res., vol. 5, no. 3, pp. 629–632, 2016.
[11] Z. Tao, Z.-B. Wang, and Q. Yu, "Finite element modelling of concrete-filled steel stub columns under axial compression," J. Constr. steel Res., vol. 89, pp. 121–131, 2013.
[12] B. Uy, "Strength of short concrete filled high strength steel box columns," J. Constr. Steel Res., vol. 57, no. 2, pp. 113–134, 2001.
[13] L.-H. Han and G.-H. Yao, "Experimental behaviour of thin-walled hollow structural steel (HSS) columns filled with self-consolidating concrete (SCC)," Thin-Walled Struct., vol. 42, no. 9, pp. 1357–1377, 2004.
[14] S. Zhang and L. Guo, "Behaviour of high strength concrete-filled slender RHS steel tubes," Adv. Struct. Eng., vol. 10, no. 4, pp. 337–351, 2007.
[15] D. Hernández-Figueirido, M. L. Romero, J. L. Bonet, and J. M. Montalvá, "Ultimate capacity of rectangular concrete-filled steel tubular columns under unequal load eccentricities," J. Constr. steel Res., vol. 68, no. 1, pp. 107–117, 2012.
[16] K. Sakino, H. Nakahara, S. Morino, and I. Nishiyama, "Behavior of centrally loaded concrete-filled steel-tube short columns," J. Struct. Eng., vol. 130, no. 2, pp. 180–188, 2004.
[17] B. Uy, "Applications, behaviour and design of composite steel-concrete structures," Adv. Struct. Eng., vol. 15, no. 9, pp. 1559–1571, 2012.
[18] Y. Yan, Z. Xing, X. Chen, Z. Xie, J. Zhang, and Y. Chen, "Axial compression performance of CFST columns reinforced by ultra-high-performance nano-concrete under long-term loading," Nanotechnol. Rev., vol. 12, no. 1, p. 20220537, 2023.
[19] J. Y. R. Liew and D. X. Xiong, "Ultra-high strength concrete filled composite columns for multi-storey building construction," Adv. Struct. Eng., vol. 15, no. 9, pp. 1487–1503, 2012.
[20] L.-H. Han, W. Li, and R. Bjorhovde, "Developments and advanced applications of concrete-filled steel tubular (CFST) structures: Members," J. Constr. steel Res., vol. 100, pp. 211–228, 2014.
[21] M. Khan, B. Uy, Z. Tao, and F. Mashiri, "Behaviour and design of short high-strength steel welded box and concrete-filled tube (CFT) sections," Eng. Struct., vol. 147, pp. 458–472, 2017.
[22] M. D. O'Shea and R. Q. Bridge, "Design of circular thin-walled concrete filled steel tubes," J. Struct. Eng., vol. 126, no. 11, pp. 1295–1303, 2000.
[23] M. Johansson and K. Gylltoft, "Mechanical behavior of circular steel–concrete composite stub columns," J. Struct. Eng., vol. 128, no. 8, pp. 1073–1081, 2002.
[24] M. Khan, B. Uy, Z. Tao, and F. Mashiri, "Concentrically loaded slender square hollow and composite columns incorporating high strength properties," Eng. Struct., vol. 131, pp. 69–89, 2017.
[25] G. Giakoumelis and D. Lam, "Axial capacity of circular concrete-filled tube columns," J. Constr. steel Res., vol. 60, no. 7, pp. 1049–1068, 2004.
[26] A. H. Varma, J. M. Ricles, R. Sause, and L.-W. Lu, "Seismic behavior and modeling of high-strength composite concrete-filled steel tube (CFT) beam–columns," J. Constr. Steel Res., vol. 58, no. 5–8, pp. 725–758, 2002.
[27] Q. Yu, Z. Tao, W. Liu, and Z.-B. Chen, "Analysis and calculations of steel tube confined concrete (STCC) stub columns," J. Constr. Steel Res., vol. 66, no. 1, pp. 53–64, 2010.
[28] E. Ellobody and B. Young, "Nonlinear analysis of concrete-filled steel SHS and RHS columns," Thin-walled Struct., vol. 44, no. 8, pp. 919–930, 2006.
[29] H.-T. Hu, C.-S. Huang, M.-H. Wu, and Y.-M. Wu, "Nonlinear analysis of axially loaded concrete-filled tube columns with confinement effect," J. Struct. Eng., vol. 129, no. 10, pp. 1322–1329, 2003.